Solid-State and Solution Structural Study of Acetylacetone-Modified Tin(IV) Chloride Used as a Precursor of SnO_2 Nanoparticles Prepared by a Sol−Gel Route

V. Briois,*,† S. Belin,† M. Zucolotto Chalaça,‡ R. H. A. Santos,§ C. V. Santilli,‡ and S. H. Pulcinelli‡

LURE, Université Paris Sud, BP34, 91898 Orsay Cédex, France, Instituto de Química, UNESP, PB 355, 14800-970, Araraquara, SP, Brazil, and Instituto de Química de São Carlos, USP, PB 780, 13560-970, São Carlos, SP, Brazil

Received January 7, 2004. Revised Manuscript Received April 6, 2004

The effect of addition of different amounts of acetylacetone (acacH) on the species formed at room temperature and after thermohydrolysis at 70 °C for 30 and 120 min of ethanolic $SnCl_4 \cdot 5H_2O$ solutions is followed by EXAFS spectroscopy at the Sn K-edge. We show that thermohydrolyzed solutions are a mixture of SnO_2 nanoparticles and soluble tin polynuclear species. The complexation of the tin molecular precursors by acetylacetonate ligands is evidenced by ^1H, ^{13}C, and ^{119}Sn NMR spectroscopy and EXAFS for a acacH/Sn ratio higher than 2. Single crystals are isolated from solution and the structure, determined by X-ray diffraction, is built up from monomeric $Cl_3(H_2O)Sn(acac) \cdot H_2O$ units bridged together by hydrogen bonding. The acacH/Sn ratio in solution controls the polycondensation of the hydrolyzed species but not the crystallite size of the SnO_2 nanoparticles (∼2 nm). Because of the major presence of chelated tin mono- and dimeric complexes in solution for acacH/Sn > 2, the condensation is almost inhibited, meanwhile the decrease of amount of chelated complexes for the acacH/Sn < 2 gives rise to an increase of the number of nanoparticles.

Introduction

Different soluble tin alkoxide[1−11] and tin halide precursors[10−19] have been used for making SnO_2 powders and thin films via the sol−gel route. The hydrolytic conversion from tin alkoxides ($Sn(OR)_4$) to metal oxides is currently under intense investigation,[1−11] aiming to introduce low-moisture-sensitive groups in the coordination sphere of tin to control the kinetics of hydrolysis, particle size, and morphology of powder and the microstructure of films. Such an approach has been successfully exploited to prepare nanoparticles of tin dioxide[3−9] and of other metal oxides with interest for ceramic applications such as TiO_2, ZrO_2, and Al_2O_3.[20−24] For example, the hydrolysis of $Ti(O^iPr)_4$ results in the formation of polydispersed 10−25-nm particles of titanium dioxide, whereas the hydrolysis of $[Ti(O^iPr)_3(acac)]_2$ (^{i}Pr = isopropyl; acacH = 2,4 pentanedione or acetylacetone) leads to the formation of a colloidal sol consisting of 5−10-nm particles and hydrolysis of $Ti(O^iPr)_2(acac)_2$ results in the formation of weakly branched polymers.[1] The hydrolysis of tetraalkoxitins leads to ill-defined

* To whom correspondence should be addressed. E-mail: briois@lure.u-psud.fr.
† Université Paris Sud.
‡ Instituto de Química.
§ Instituto de Química de São Carlos.

(1) Hampden-Smith, M. J.; Wark, T. A.; Brinker, C. J. *Coord. Chem. Rev.* **1992**, *112*, 81.
(2) Hampden-Smith, M. J.; Wark, T. A.; Rheingold, A.; Huffman, J. *Can. J. Chem.* **1991**, *69*, 121.
(3) Armelao, L.; Ribot, F.; Sanchez, C. *Mater. Res. Soc. Symp. Proc.* **1996**, *435*, 387.
(4) Gamard, A.; Jousseaume, B.; Toupance, T.; Campet, G. *Inorg. Chem.* **2000**, *38*, 4671.
(5) Gamard, A.; Babot, O.; Jousseaume, B.; Rascle, M. C.; Toupance, T.; Campet, G. *Chem. Mater.* **2000**, *12*, 3419.
(6) Toupance, T.; Babot, O.; Jousseaume, B.; Vilaça, G. *Chem. Mater.* **2003**, *15*, 4691.
(7) de Monredon, S.; Cellot, A.; Ribot, F.; Sanchez, C.; Armelao, L.; Gueneau, L.; Delattre, L. *J. Mater. Chem.* **2002**, *12*, 2396.
(8) Eychenne-Baron, C.; Ribot, F.; Sanchez, C. *J. Organomet. Chem.* **1988**, *567*, *1*31.
(9) Guliver E. C.; Garvey, J. W.; Wark, T. A.; Hampden-Smith, M. J.; Datye, A. *J. Am. Ceram. Soc.* **1991**, *74*, 1091.
(10) Chandler, C. D.; Fallon, G. K.; Koplick, A. J.; West, B. O. *Aust. J. Chem.* **1987**, *4*, 1427.
(11) Verdenelli, M.; Parola, S.; Hubert-Pfalzgraf, L. G.; Lecocq, S. *Polyhedron* **2000**, *19*, 2069.
(12) Miller, G. A.; Schlemper, E. O. *Inorg. Chim. Acta* **1978**, *30*, 131.
(13) Jones, R. W., Jr.; Fay, R. C. *Inorg. Chem*, **1973**, *12*, 2599.
(14) Ocaña, M.; Matijevic, E. *J. Mater. Res.* **1990**, *5*, 1083.
(15) Aegerter, M. A.; Reich, A.; Ganz, D.; Goebbert, C.; Putz, J.; Krajewski, T. *J. Non Cryst. Solids* **1997**, *218*, 123.
(16) Santos, L. R. B.; Larbot, A.; Persin, M.; Santilli, C. V.; Pulcinelli, S. H. *J. Sep. Purif. Technol.* **2001**, *22&23*, 17.
(17) Rizzato, A. P.; Santilli, C. V.; Pulcinelli, S. H.; Messaddecq, Y. *J. Non Cryst. Solids* **1999**, *256&257*, 154.
(18) Rizzato, A. P.; Broussous, L.; Santilli, C. V.; Pulcinelli, S. H.; Craievich, A. F. *J. Non Cryst. Solids* **2001**, *284*, 61.
(19) Broussous, L.; Santilli, C. V.; Pulcinelli, S. H.; Craievich, A. F. *J. Phys. Chem. B* **2002**, *106*, 2855.
(20) Sanchez, C.; Soler-Illia, G. J. de A. A.; Ribot, F.; Lalot, T.; Mayer, C. R.; Cabuil, V. *Chem. Mater.* **2001,** *13*, 3061.
(21) Scolan, E.; Sanchez, C. *Chem. Mater.* **1998**, *10*, 3217.
(22) Hoebbel, D.; Reinert, T.; Schmidt, H. *J. Sol-Gel Sci., Technol.* **1997**, *10*, 115.
(23) Maeda, K.; Mizukami, F.; Niwa, S.; Toba, M.; Watanabe, M.; Masuda, K. *J. Chem. Soc., Faraday Trans.* **1992**, *88*, 97.
(24) Kaneko, E. Y.; Pulcinelli, S. H.; Teixeira da Silva, V.; Santilli, C. V. *J. Appl. Catal.* **2002**, *235*, 71.

10.1021/cm040141q CCC: $27.50
Published on Web 09/01/2004

aggregates (200−250 nm) of primary particles (35−85 nm),[9] while the lowering of the functionality of alkoxitin precursor by complexation with weak hydrolyzable groups, such as β-diketones, leads to the formation of well-defined tin dioxide nanoparticles with average size of 6−8 nm.[6] The list of organic modified tin alkoxide by direct attachment of organic groups via C−Sn bonds or partially complexed with β-diketones is very large[1−11] (see also references therein), but systematic investigation of the structure of species obtained in the initial step of hydrolyses is relatively sparse.[1−6] The single-crystal structures of organic-modified tin alkoxide precursors were reported, including as example the β-diketones $[Sn(O^iPr)_3(acac)]_2$,[10] $Sn(OEt)_2(\eta^2\text{-acac})_2$, and $Sn_4(\mu_3\text{-}O)_2(\mu_2\text{-}OEt)_4(OEt)_6(\eta^2\text{-acac})_2$ [11] (Et = ethyl). However, in the case of acac-modified tin halides, only the $Cl_2Sn(acac)_2$ has a known single-crystal structure.[12]

As metal alkoxide precursors are expensive, extremely sensitive to heat, moisture, and light, and their preparation is time-consuming,[1] soluble tin halide precursors could be more appropriate for industrial applications; many papers report the SnO_2 sol−gel synthesis from tin chloride solutions.[13−19] The clear sol obtained by this way was used to prepare conductive and transparent films,[15] ultrafiltration membranes,[16] and anticorrosion coatings.[17] The use of $SnCl_4$ ethanolic solution instead of aqueous solutions results in a mixture of SnO_2 nanoparticles and unhydrolyzed soluble species.[18] The precipitation of soluble species during drying of films leads to reduction of porosity from 50 to 30% with respect to aqueous sol derivative coatings.[18] Recently, we have shown[19] that the relative amount of unhydrolyzed species can be tuned by changing the [acacH]/[Sn] ratio in the initial precursor solution. This feature can be useful to control the porosity of SnO_2 films.

This paper falls under our general effort to improve the microstructural property of the SnO_2 coatings by controlling the chemistry of the sol−gel route. The objectives of this article are the determination of the solution and solid-state structure (EXAFS, SCXRD, and NMR data) of acac-modified tin tetrachloride precursor and of the hydrolysis products. Furthermore, we tried to get more quantitative information on the effect of the nominal complexing ratio [acacH]/[Sn] on the hydrolytic stability of the soluble complexes and on the SnO_2 nanocrystallite size.

Experimental Section

Preparation of Samples. The precursor solution was prepared by dissolving 0.09 mol/L tin tetrachloride pentahydrate in absolute ethanol. Different amounts of acetylacetone, $C_5H_8O_2$ (noted acacH), were added at room temperature (RT) to the solution to yield [acacH]/[Sn] nominal complexing ratios of 0.0, 0.5, 1.0, 2.0, 4.0, and 6.0. They are referred to as Ac0, Ac05, Ac1, Ac2, Ac4, and Ac6, respectively. The nominal hydrolysis ratio of alcoholic solution prepared from pentahydrate tin tetrachloride ($h = [H_2O]/[Sn] = 5$) was adjusted by dropwising addition of distilled water to yield $h = [H_2O]/[Sn] = 105$. The acid (pH ≅1) solutions were put into reflux apparatus and the thermohydrolysis was carried out at 70.0 ± 0.5 °C for 120 min, giving rise to transparent and stable sols. After that, the suspensions were cooled to RT, put inside acetylcellulose membranes tubing (12−14 000 M_W), and then submitted to static dialysis to eliminate as much as possible unhydrolyzed complex and other soluble species. The colloidal particles were isolated by freeze-drying at −5 °C and pressure of ∼1 μmHg.

NMR, Mass Spectroscopy Characterizations, and Elemental Analysis. NMR solution analyses were performed on a Varian Inova 300 Unity spectrometer. ^{1}H NMR spectra were recorded at 300 MHz, and ^{13}C NMR were obtained at 75.42 MHz. Chemical shifts were referenced to tetramethylsilane using the proton impurities of the deuterated solvent. ^{119}Sn NMR spectra were recorded at 111.85 MHz, and chemical shifts are quoted relative to $(CH_3)_4Sn$, using $SnSO_4$ aqueous solution ($\delta = -909$ ppm) as a secondary external reference.[25] NMR characterizations were performed on Ac6 solutions with $h = 5$ and $h = 105$ before thermohydrolysis at 70 °C. After removal at RT under vacuum of volatile components, solid compounds were obtained in both cases, labeled complexes C0−Ac6 and C100−Ac6, respectively. The prolonged aging (two months) of C100−Ac6 in the liquor mother (acacH in excess) gives rise to the formation of colorless prismatic single crystals. The compounds C0−Ac6 and C100−Ac6 and the single crystals so obtained were completely soluble in CD_3OD and analyzed by multinuclear NMR (^{1}H, ^{13}C, ^{119}Sn) spectroscopy. For microanalysis (C, H) the C0−Ac6 and C100−Ac6 powders were dried in a vacuum to constant weight (25 °C, ∼0.01 Torr). Elemental analyses were performed with a Perkin-Elmer model CHNS-O 1110 instrument.

Electrospray mass spectra (ESI-MS) were obtained with a Platform II single quadrupole mass spectrometer (Micromass) using an acetonitrile/H_2O (1:1) mobile phase. Methanol solutions of the compounds were injected directly into the spectrometer via a Rheodine injector equipped with a 10-μL loop. A LC pump Shimadzu 10-AD delivered the solutions to the vaporization nozzle of the electrospray ion source at flow rate of 10 μL min^{-1}. Nitrogen was used both for drying and for nebulization with flow rates of approximately 200 and 20 mL min^{-1}, respectively.

Single-Crystal X-ray Diffraction (SCXRD). Colorless prismatic single crystal was measured on an Enraf-Nonius CAD-4 diffractometer with graphite-monochromated Mo Kα ($\lambda = 0.710\ 73$ Å) radiation working at RT. Unit-cell parameters and orientation matrix for data collection were obtained from least-squares refinement using the setting angles of 25 reflections in the θ range 14.78−18.20°. Ψ-scan absorption correction[26] was applied. The structure was solved by the Patterson and difference Fourier methods using the WinGX System.[27] The structure models were refined by a full-matrix least-squares procedure on F^2 by means of SHELXL-97.[28] In the refinement procedure, all non-hydrogen atoms were treated anisotropically. The hydrogen atoms of the water were obtained in the Fourier difference map and refined; the carbon−hydrogen atoms were located in their ideal positions and not refined. All isotropic hydrogen thermal displacement parameters were set as 1.3 times the isotropic equivalent thermal displacement of the attached atom.

EXAFS Measurements. EXAFS measurements were made at LURE using the DCI storage ring (1.85 GeV and 300 mA). The EXAFS data were collected at the Sn K-edge (30 keV), in transmission mode, on the EXAFS IV spectrometer[29] using a two-crystal Ge (400) monochromator. The flux intensities before and after the sample were measured by means of ionization chambers filled with krypton. The EXAFS spectra were recorded within a 1200-eV energy range with 4-eV steps and 2-s accumulation time per energy. Solutions were characterized at RT, using a liquid cell with Kapton windows and an optical path length of ∼15 mm. The solutions before heating with $h = 105$ were measured during the first hour after the addition of water. Freeze-dried powders (40 mg) were mixed with 30 mg of cellulose and prepared as pellets. Crystalline

(25) Burke, J. J.; Lauterbur, P. C. *J. Am. Chem. Soc.* **1961**, *83*, 326.
(26) North, A. C. T.; Phillips, D. C.; Mathews, F. S. *Acta Crystallogr.* **1968**, *A24*, 351.
(27) Farrugia, L. J. *J. Appl. Crystallogr.* **1999**, *32*, 837.
(28) Sheldrick, G. M. *Programs for Crystal Structure Analysis, Release 97-2*; Institüt für Anorganische Chemie der Universität: Göttingen, Germany, 1998.
(29) Sainctavit, Ph.; Petiau, J.; Manceau, A.; Rivallant, R.; Belakhovsky, M.; Renaud, G. *Nucl. Inst. Methods Phys. Res.* **1988**, *A273*, 423.

SnO_2 and dichlorobis(2,4-pentanedionato)tin(IV), $Cl_2Sn(acac)_2$, furnished by Sigma Aldrich, were used as EXAFS references.

EXAFS Data Analysis. The EXAFS data analysis was processed using the procedure fully described in an earlier paper[30] by using the chain of programs developed by Michalowicz[31] and briefly summarized below. For the atomic absorption removal $\mu_0(E)$, the total absorption curve, $\mu(E)$, above the edge was fitted by a cubic spline function of the fifth order. The EXAFS signal $\chi(E)$ was obtained from a normalization using the Heitler numerical procedure[32] and a subsequent transformation of the energy to wavenumber scale (k). The $k^3\chi(k)$ weighted EXAFS signal was then Fourier transformed to R distance space over $\sim$11 Å^{-1} (3.8−15.0 Å^{-1}) using a Kaiser apodization window with $\tau = 3$. The contributions of the various shells of neighbors were extracted from the so-obtained pseudo-radial distribution function (PRDF) by a back Fourier transform in R space.

Simulations need the knowledge of amplitude and phase functions for three types of backscattering atoms: oxygen and chlorine atoms for the first coordination shell and tin atoms for the second nearest neighbors. Oxygen backscattering functions were extracted from the crystalline SnO_2 reference after inverse Fourier transform of the first peak of the PRDF and setting $N = 6$ as oxygen coordination number, $R = 2.06$ Å as Sn−O distance in the first coordination shell, and $\sigma^2 = 3.6$ 10^{-3} Å^2 as Debye−Waller factor for this shell. For chlorine and tin backscattering atoms, theoretical phase and amplitude functions were calculated in the curved wave approximation by using the FeFF6 code developed by Rehr and co-workers[33] and tested on the dichlorobis(2,4-pentanedionato)tin(IV), $Cl_2Sn(acac)_2$,[12] and crystalline SnO_2[34] references, respectively. In $Cl_2Sn(acac)_2$,[12] the tin atom is in a distorted octahedral coordination with two chlorine atoms at 2.345 Å and four oxygen atoms of the two bidentate acetylacetonate ligands at 2.055 Å. Errors in the structural parameters were calculated from the standard deviation of each data point defined by the relation, $s(k) = 1/k^2$.[35]

Results

Effect of AcacH/Sn Ratio on the Structure of Freeze-Dried Products. Figure 1 shows the PRDFs around Sn atoms obtained for the SnO_2 crystalline reference and the powdered samples obtained after thermohydrolysis, dialysis, and subsequent freeze-drying. As for the polycrystalline SnO_2 reference, two main peaks ranging between 1 and 4 Å are observed on the PRDFs of the powders. The first peak is related to the first coordination shell of oxygen atoms at 2.06 Å, and the second broad one is related to the main Sn contributions at 3.19 and 3.72 Å. They are characteristic of the cassiterite type structure.[34] Peaks at $R > 4$ Å correspond to the tin contributions at longer distances in the cassiterite network. It is noteworthy that the intensity of the PRDFs of the different powders does not depend on the acacH/Sn ratio. As a consequence, the structural parameters determined by a least-squares fitting procedure to simulate the first and second peaks of these PRDFs were found invariant, whatever the acacH/Sn ratio in starting solution. The structural parameters so

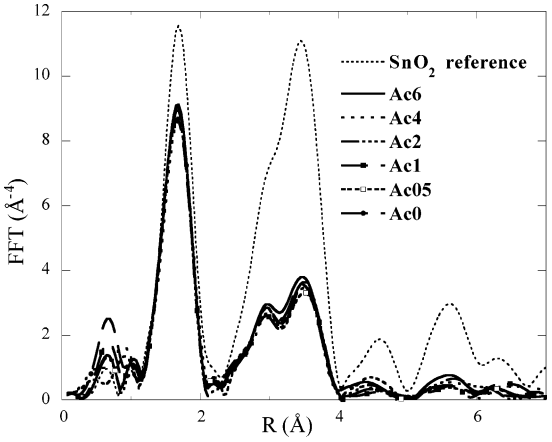

Figure 1. Pseudoradial distribution functions around Sn of the SnO_2 crystalline reference and of the powdered freeze-dried samples as a function of the acacH/Sn ratio.

obtained were 6.0 ± 0.3 oxygen atoms at 2.06 ± 0.01 Å and 1.6 ± 0.2 and 4.8 ± 0.4 tin atoms at 3.20 ± 0.01 and 3.73 ± 0.01 Å, respectively. The Debye−Waller factors were found at 3.6 × 10^{-3} ± 10^{-4} Å^2 for the oxygen and first tin nearest neighbors and 4.9 × 10^{-3} ± 10^{-4} Å^2 for the second tin nearest neighbors. The drastic reduction of the tin coordination numbers in second nearest neighbors for the freeze-dried samples compared to the polycrystalline SnO_2 reference (2 Sn at 3.19 Å and 8 Sn at 3.72 Å) is due to the nanometric size effect of the colloidal particles.[30,36] Indeed the important contribution to the total EXAFS signal of absorbing atoms located at the surface of nanocrystallites with fewer cationic nearest neighbors induces a significant reduction of the mean coordination number for cationic−cationic contribution compared to the value for bulk materials containing well-developed crystallites. The nanocrystalline size of the different samples estimated according to the recurrence formula established in ref 30 is $\sim$2.3 ± 0.3 nm whatever the acacH/Sn ratio. These results indicate that the addition of acac as complexing ligand has an insignificant effect on the control of particle size growth.

Effect of AcacH/Sn Ratio on the Thermohydrolysis of the Solutions. The evolution of the PRDFs for Ac0, Ac05, Ac1, Ac2, Ac4, and Ac6 solutions before and after 120 min of thermohydrolysis are presented in Figure 2a−f, respectively. This figure reports also the PRDFs corresponding to the solutions with hydrolysis rate $h = 5$. Solutions with $h = 5$ present a single intense peak around 2.0 Å with a faintly marked shoulder around 1.5−1.6 Å. The intensity of this peak clearly decreases with the amount of acacH in solution. This evolution could account for the complexation of Sn by acetylacetonate ligands. Solutions with $h = 105$ are characterized by two maximums located at 1.6 and 2.0 Å, respectively. Quantitative analysis of these contributions shows that the one at 1.6 Å is due to oxygen backscattering atoms located at 2.07 ± 0.01 Å from Sn whereas the one at 2.0 Å is related to a chlorine contribution located at 2.37 ± 0.01 Å from Sn. For sake of clarity, the Sn−O and Sn−Cl related contributions are only indicated in Figure 2a and f.

(30) Briois, V.; Santilli, C. V.; Pulcinelli, S. H.; Brito G. E. S. *J. Non Cryst. Solids* **1995**, *191*, 17.
(31) Michalowicz, A. *EXAFS pour le Mac, Logiciels pour la Chimie*; Société Française de Chimie: Paris, 1991; p 102.
(32) Heitler, W. *Quantum theory of radiation*, 3rd ed.; Oxford University Press: 1954; and references therein. Lengeler, B.; Eisenberger, P. *Phys. Rev. B* **1980** *21*, 4507.
(33) Zabinsky, S. I.; Rehr, J. J.; Ankudinov, A.; Albers, R. C.; Eller, M. J. *Phys. Rev. B* **1995**, *52*, 2995.
(34) Baou, W. H. *Acta Crystallogr.* **1956**, *9*, 515.
(35) Lytle, F. W.; Sayers, D. E.; Stern, E. A. *Physica B* **1989**, *158*, 701.
(36) Briois, V.; Pulcinelli, S. H.; Santilli, C. V. *J. Mater. Sci. Lett.* **2001**, *20*, 555

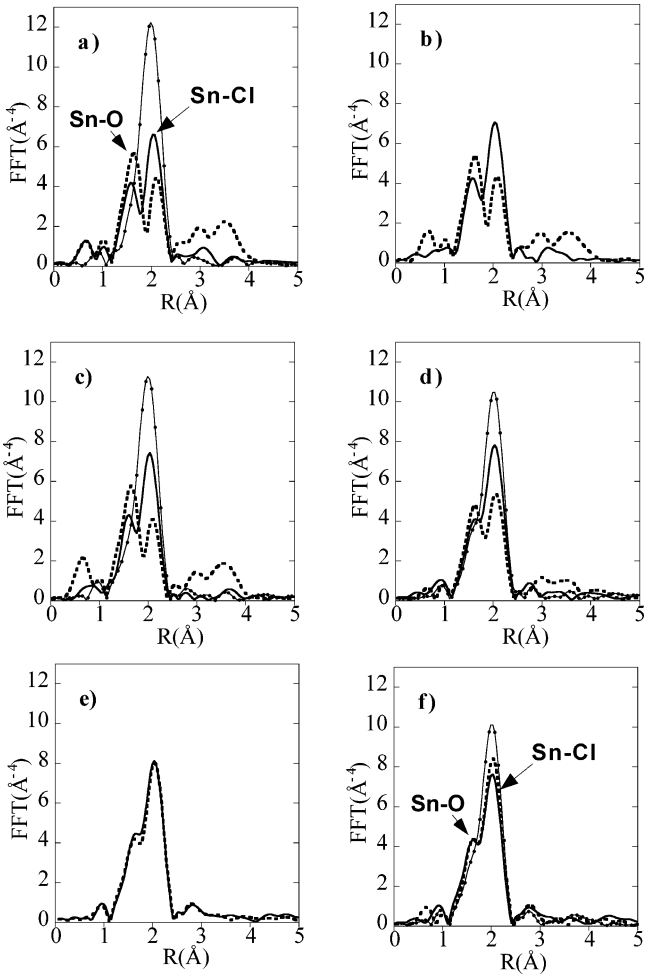

Figure 2. Pseudoradial distribution functions around Sn of the different solutions with $h = 105$ before (full line) and after (dashed line) thermohydrolysis at 70 °C during 120 min: (a) Ac0, (b) Ac05, (c) Ac1, (d) Ac2, (e) Ac4, and (f) Ac6. For Ac0, Ac1, Ac2, and Ac6, the PRDF's for ethanolic solutions with $h = 5$ are also reported in full dotted line.

The comparison of the PRDFs of the solutions with $h = 105$ before thermohydrolysis shows two distinct behaviors with respect to the complexation depending on the acacH/Sn ratio. For acacH/Sn ≥ 2, the intensities of the oxygen and chlorine contributions do not change with the acacH content and the oxygen contribution appears as a pronounced shoulder at the left side of the chlorine contribution. For acacH/Sn < 2, the splitting of the oxygen and chlorine contributions is enhanced and the relative intensity of the chlorine contribution increases with the acacH amount. This behavior suggests that the local order around tin after the addition of 2 equivalents of acacH with respect to Sn is insensitive to further increase of acacH content in the reaction bath.

Comparing now the PRDFs of the different solutions before and after thermohydrolysis, no significant change for the Ac4 and Ac6 solutions (Figure 2e and f) is observed, whereas for acacH/Sn ≤ 2, important changes in the relative intensity of the two main peaks are observed (Figure 2a−d). In this case, the thermohydrolysis leads to an increase of the intensity of the first peak related to the oxygen contribution and to a decrease of the intensity of the second one related to the chlorine contribution. This effect is stronger as the acacH content decreases, evidencing the substitution of Sn−Cl by the Sn−O bond due to the hydrolysis or complexation reactions, or both. This exchange decreases as the acacH/Sn ratio increases up to 2, indicating that either the thermohydrolytic stability of the precursors or the number of acac ligands reaches a maximum for acacH/Sn ≈ 2. Furthermore, contributions at longer distances ($R > 2.2$ Å) are observed after the hydrolysis at 70 °C, indicating the existence of a medium-range order around Sn due to condensation reactions. As observed in Figure 3 for different thermohydrolysis times carried out for Ac0 and Ac1, the longer the hydrolysis time, the higher the intensities of the peaks relative to the oxygen and tin atom contributions, indicating that the condensation reactions progress with time. It is also noteworthy that at the early stage of thermohydrolysis ($t = 30$ min) the intensity of the tin contributions is higher for solutions without acacH than with acacH, indicating that the addition of acacH delays the condensation reactions. The structural parameters obtained by a least-squares fitting procedure to simulate the peaks in the range 0.9−2.4 Å of the PRDFs displayed in Figure 2 are gathered in Table 1. For all these solutions, the fitting procedure is based on a two-shells procedure involving oxygen and chlorine backscattering atoms. For solutions with $h = 5$, which are characterized by a single broad peak, the best simulations are obtained by considering a two-shells model with 0.8−1.7 oxygen atoms at 2.08 ± 0.01 Å and 4.4−3.7 chlorine atoms at 2.37 ± 0.01 Å. We note a concomitant decrease of the coordination number for the chlorine shell and an increase of the coordination number for the oxygen shell when the acacH amount in the reaction bath increases. This could be attributed to a partial substitution of chlorine atoms and water or EtOH ligands by acac ligands. Then the oxygen contribution for Ac1, Ac2, and Ac6 before the addition of water partially arises from the complexation of Sn by acac ligands.

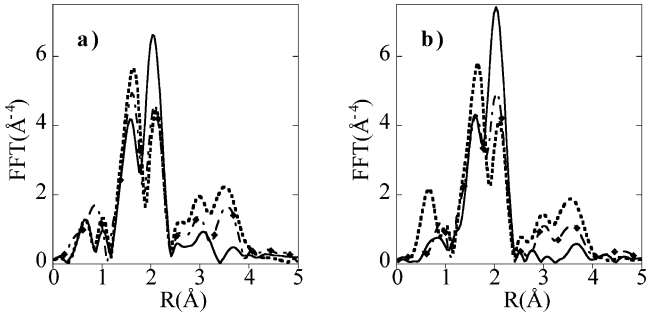

Figure 3. Kinetics of thermohydrolysis for (a) Ac0 and (b) Ac1. The PRDFS correspond to $t = 0$ (full line), 30 (dot and dashed lines), and 120 min (dashed line) of thermohydrolysis at 70 °C.

The expected chelation of tin by acetylacetonate ligands is strongly suggested by the EXAFS results. Actually, this chelation is clearly evidenced by the presence of carbon atoms as second neighbors of tin (peak ∼2.7 Å) for solutions prepared with acacH/Sn ≥ 2 as presented in Figure 2. This carbon contribution was also observed in the experimental PRDF of the reference compound $Cl_2Sn(acac)_2$ and of $Cl_3(H_2O)Sn(acac)\cdot H_2O$ single crystal isolated here. These spectra, presented in Figure 4, were successfully reproduced by ab initio simulations performed with the FeFF6[33] and FeFFIT[37]

Table 1. Structural Parameters Obtained from the Filtered EXAFS Signal (Filtered *R* Range = 0.9−2.4 Å) for the Different Ethanolic Solutions of Tin(IV) Chloride Modified by acaH before ($h = 105$, $t = 0$ min) and after ($h = 105$, $t = 120$ min) Thermohydrolysis[a]

samples before thermohydrolysis ($t = 0$ min)	*N*	*R* (Å)	χ^2	samples after thermohydrolysis ($t = 120$ min)	*N*	*R* (Å)	$\chi 2$
$Cl_2Sn(acac)_2$ ref	4 O	2.055	1.57				
	2 Cl	2.345					
Ac0, $h = 5$	0.8 ± 0.4 O	2.08	1.09				
	4.4 ± 0.2 Cl	2.37					
Ac0, $h = 105$	3.3 ± 0.3 O	2.06	0.94	Ac0, $h = 105$	4.2 ± 0.6 O	2.07	0.98
	2.6 ± 0.2 Cl	2.37			2.0 ± 0.3 Cl	2.37	
Ac05, $h = 105$	3.2 ± 0.1 O	2.07	1.05	Ac05, $h = 105$	4.5 ± 0.6 O	2.08	1.36
	2.7 ± 0.1 Cl	2.36			1.9 ± 0.3 Cl	2.37	
Ac1, $h = 5$	1.1 ± 0.5 O	2.09	0.41				
	4.1 ± 0.3 Cl	2.37					
Ac1, $h = 105$	3.0 ± 0.2 O	2.06	0.91	Ac1, $h = 105$	4.4 ± 0.2 O	2.08	2.86
	2.9 ± 0.2 Cl	2.36			2.2 ± 0.2 Cl	2.37	
Ac2, $h = 5$	1.6 ± 0.5 O	2.07	1.52				
	3.8 ± 0.3 Cl	2.38					
Ac2, $h = 105$	3.0 ± 0.2 O	2.07	0.91	Ac2, $h = 105$	3.9 ± 0.2 O	2.08	0.39
	3.2 ± 0.2 Cl	2.37			2.3 ± 0.2 Cl	2.37	
Ac4, $h = 105$	3.0 ± 0.1 O	2.07	1.59	Ac4, $h = 105$	3.0 ± 0.2 O	2.06	1.37
	3.1 ± 0.1 Cl	2.36			3.0 ± 0.2 Cl	2.37	
Ac6, $h = 5$	1.7 ± 0.5 O	2.08	0.88				
	3.7 ± 0.3 Cl	2.37					
Ac6, $h = 105$	3.1 ± 0.2 O	2.06	1.08	Ac6, $h = 105$	2.8 ± 0.1 O	2.07	1.04
	2.8 ± 0.2 Cl	2.37			3.2 ± 0.1 Cl	2.36	

[a] The effect of addition water is reported with the structural parameters for solutions with $h = 5$. *N* and *R* are the running parameters whereas the Debye−Waller factors were fixed to 4.9×10^{-3} Å^2 in both subshells. The reliability of the fit is given by the χ^2 parameter defined by $\chi^2 = (N_{ind}/N_{pts})\sum_{i=1}^{i=N_{pts}}(1/s(k)^2)[k\chi_{exp}(k) - k\chi_{th}(k)]^2$, where N_{ind} is the number of independent points, N_{pts} is the number of data points, and $s(k)$ is the standard deviation defined by $s(k) = 1/k^2$.

codes based on the crystallographic structure of $Cl_2Sn(acac)_2$[12] and of $Cl_3(H_2O)Sn(acac)\cdot H_2O$ described in the next section. Distances were fixed at the crystallographic values,[12,13] and only the Debye−Waller factors of the different single and double scattering paths involving the atoms located at $R \leq 3.4$ Å from Sn were refined. These simulations unambiguously identify the peak around 2.7 Å in the PRDFs as arising from the carbon atoms of the acetylacetonate ligand.

Before thermohydrolysis but when water is added ($h = 105$), the first coordination shell is described in average by 3.0 oxygen atoms at 2.06 ± 0.01 Å and 3.0 chlorine atoms at 2.37 ± 0.01 Å, whatever the acacH content (Table 1). Then the addition of water leads to a substantial modification of the composition of the two subshells. The coordination number of the oxygen shell, N_{Sn-O}, increases whereas the coordination number of the chlorine shell, N_{Sn-Cl}, decreases.

Taking into account the error bars on the determination of the coordination number, the N_{Sn-O} and N_{Sn-Cl} numbers for Ac4 and Ac6 ($h = 5$) are invariant before and after thermohydrolysis (Table 1). This confirms that the change of the local order around Sn by thermohydrolysis is very small for acacH/Sn > 2. On the other hand, for acacH/Sn ≤ 2, N_{Sn-O} increases 1.0−1.5 atom, whereas N_{Sn-Cl} decreases 0.6−0.9 atom. The composition after thermohydrolysis of both subshells for Ac05 and Ac1 is equal to that for Ac0 within the error bars.

Structure of Isolated C0−Ac6 and C100−Ac6 Complexes and of $Cl_3(H_2O)Sn(acac)\cdot H_2O$ Single Crystal. In the ^{1}H and ^{13}C NMR spectra of the Sn complex C0−Ac6 dissolved in CD_3OD, the signals of chelating acac were clearly observed besides the presence of that ones belonging to free acacH in excess, which was not totally removed during the preparation for NMR characterizations. Before hydrolysis (complex C0−Ac6), the ^{1}H NMR spectrum at RT shows two singlets at 5.91 and 2.17 ppm attributed to the CH and methyl of the acac ligand. Moreover, two weak peaks located at 5.86 and 2.14 ppm are also observed, suggesting the presence of acac coordinated to another tin species. In addition, ^{13}C NMR spectrum exhibits peaks for CH_3, CH, and CO of the chelating ligand at 27.79, 103.12, and 197.81 ppm, respectively, and less intense peaks corresponding to a secondary species observed at 27.63, 102.65, and 197.01 ppm. In this spectrum, the satellites of ^{13}C−^{119}Sn scalar couplings could be detected: 30 ($^3J_{methyl}$), 94 ($^3J_{CH}$), and 44 Hz ($^2J_{CO}$). The ^{119}Sn NMR spectrum of the complex C0−Ac6, presented in Figure 5a, displays a single major resonance with a chemical shift at −616 ppm together with much less intense resonance at −635, −606, −628, and −652 ppm. The origin of these three later low-intensity second resonances marked by arrows at the ^{119}Sn NMR spectrum can be attributed to species originated from $SnCl_4$ in methanol solution. This statement is based on the observation that the ^{119}Sn NMR spectrum of the pure $SnCl_4\cdot 5H_2O$ in methanol shows three very broad signals with the same chemical shifts. Correlation of ^{119}Sn chemical shift values with tin coordination numbers were previously reported,[10,11,38] and accordingly, the chemical shift at −616 ppm of compound C0−Ac6 is consistent with 6-fold coordinated species. Despite the

(37) Newville, N.; Ravel, B.; Haskel, D.; Rehr, J. J.; Stern, E. A.; Yacoby, Y. *Physica B* **1995**, *208&209*, 154.

(38) Hani, R.; Geanangel, R. A. *Coord. Chem. Rev.* **1982**, *44*, 229.

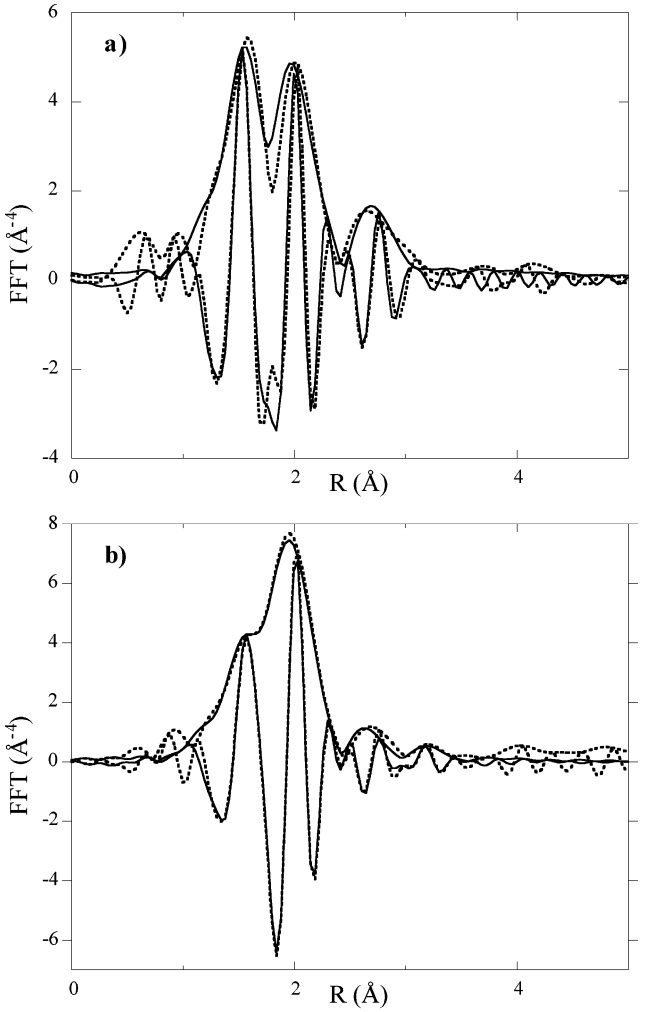

Figure 4. FeFFIT simulations of the EXAFS spectra of (a) the $Cl_2Sn(acac)_2$ reference and (b) the $Cl_3(H_2O)Sn(acac)\cdot H_2O$ single-crystal according to their crystallographic structures. The structural parameters used in the simulation of the Cl_2-$Sn(acac)_2$ compound are $N_O = 4$ at 2.055 Å with $\sigma^2 = 3.6\ 10^{-3}$ Å^2, $N_{Cl} = 2$ at 2.345 Å with $\sigma^2 = 2.5\ 10^{-3}$ Å^2, $N_C = 4$ at 2.98 Å, and $N_C = 2$ at 3.33 Å with $\sigma^2 = 3.6\ 10^{-3}$ Å^2. Those used in the simulation of the $Cl_3(H_2O)Sn(acac)\cdot H_2O$ single crystal are reported in Table 4, presented as Supporting Information.

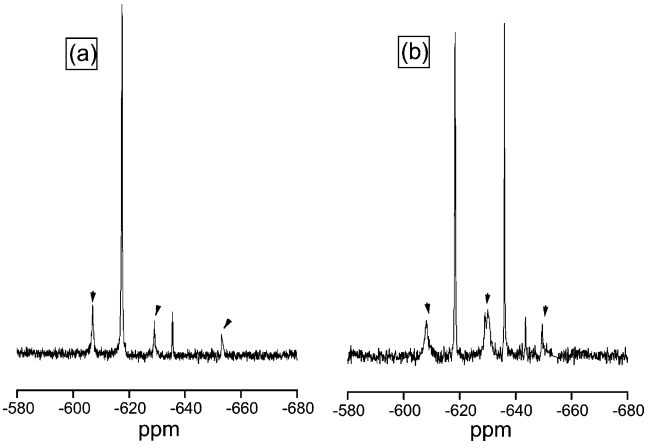

Figure 5. ^{119}Sn NMR spectra of C0−Ac6 (a) and C100−Ac6 (b) complexes recorded in CD_3OD solution at RT. Arrows indicate peaks related to $SnCl_4\cdot 5H_2O$ in methanol.

observed peak broadness (40 Hz for the peak at 616 ppm), indicative of exchange processes involving isomeric species for the complex, the identification of these isomers is uncertain. Examination of the effect of temperature and concentration on the ^{119}Sn spectra coupled to molecular weight studies could improve considerations on the origin of these resonances. The ESI-MS data revealed the $[Cl_3(H_2O)Sn(acac)]^+$ (*m*/*z* 341) molecular ion besides $[M^+ - H_2O]$ fragment (*m*/*z* 323). These spectroscopic data strongly suggest that the complex C0−Ac6 exists in solution as $Cl_3(H_2O)Sn(acac)$. Furthermore, C = 15.5 wt % and H = 2.8 wt % were found in elemental microanalysis, which are in reasonable agreement with the stoichiometry of this monochelate complex (Anal. Calcd of $Cl_3(H_2O)Sn(acac)$: C =17.5 wt %, H= 2.6 wt %). The difference between the expected and the measured carbon and hydrogen contents is indicative of the presence of a minor amount of secondary tin species. The local tin environment of the predominant species can be therefore constituted of one acac ligand, a water molecule, and three chlorine atoms arranged in an octahedral symmetry. This result is in agreement with the average coordination number determined by EXAFS for the Ac6, $h = 5$ solution. Nevertheless, the first coordination sphere around tin was described (Table 1) for this solution by 3.7 ± 0.3 chlorine atoms and 1.7 ± 0.5 oxygen atoms belonging to acac ligand. The difference between both structural descriptions could result from the fact that the Ac6, $h = 5$ solution was characterized by EXAFS just after addition of acacH. Then the formation of the $Cl_3(H_2O)$-$Sn(acac)$ compound may occur at an early stage during the concentration of the initial solution.

The presence of chelating acac on tin nuclei in complex was also pointed out by ^{1}H and ^{13}C NMR spectra of C100−Ac6 sample obtained after addition of water at RT, which presents the same peaks observed for C0−Ac6. However, the intensity of the lines corresponding to the secondary species increases and becomes as intense as that of dominant resonance initially verified for C0−Ac6. The ratio between integrated areas of peaks located at 5.86 and 5.91 ppm in ^{1}H NMR increases from 0.10 to 0.77 after addition of water. This behavior was also noted in the ^{13}C NMR spectrum and is clearly illustrated in the ^{119}Sn NMR spectrum displayed in Figure 5b. In this spectrum, the ratio between peaks located at −616 and −635 ppm increases from 0.08 (Figure 5a) to 0.77 after addition of water (Figure 5b). The peak at −635 ppm is in good agreement with the chemical shift reported[10] for the bis-chelate complex $Cl_2Sn(acac)_2$. This behavior is analogous to the equilibrium between the dimer $[Sn(acac)(OR)_3]_2$ and the monomer $Sn(acac)_2(OR)_2$ verified by Chandler et al.[10] in which a new ^{119}Sn resonance placed at a more negative chemical shift continuously increases when monomer is converted into dimeric species. The mass spectral data obtained in the ESI mode reveal the presence of $[Cl_3$-$Sn(acac)]_2^+$ (*m*/*z* 645) molecular ion besides fragment *m*/*z* 446 $[M^+ - 2acac]$ of the molecule mixed with those corresponding to $Cl_3(H_2O)Sn(acac)$ fragments.

The prolonged aging (two months) of C100−Ac6 in the liquor mother (acacH in excess) gives rise to the formation of colorless prismatic crystals. The ^{119}Sn NMR spectrum of these crystals dissolved in CD_3OD presents a single resonance located at the same chemical shift (−616 ppm) of the most intense peak verified in Figure

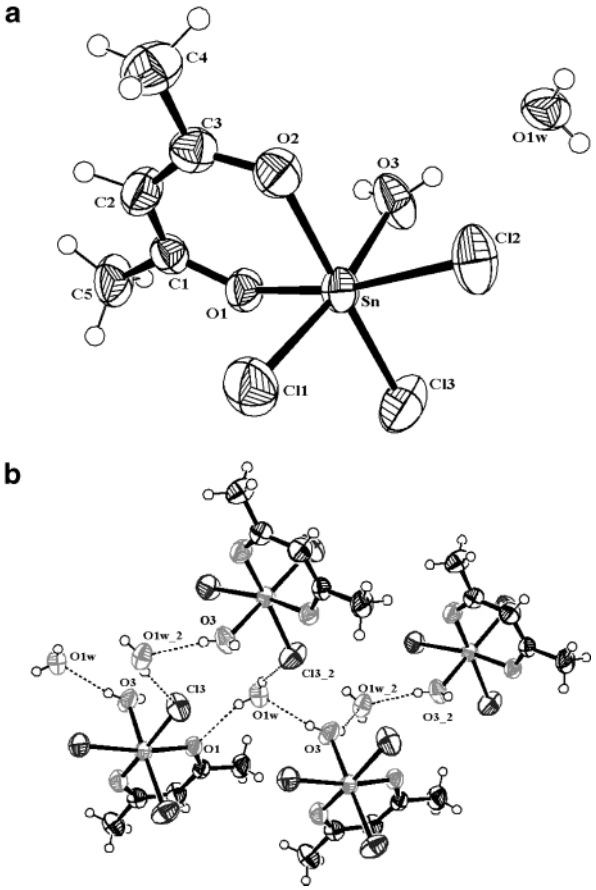

Figure 6. ORTEP plots, with 50% of thermal ellipsoid probability, of the (a) molecular geometry and atom labeling and (b) crystal structure showing hydrogen bonding for trichlorohydro(2,4-pentanedionato)tin(IV) monohydrate, $Cl_3(H_2O)Sn(acac)\cdot H_2O$.

5a. Thus, only the dominant complex formed before water addition, which we assumed as being $Cl_3(H_2O)$-Sn(acac), seems responsible for making these crystals. In fact, the crystal structure, determined by X-ray diffraction, consists of $Cl_3(H_2O)Sn(acac)\cdot H_2O$ units (Anal. Calcd for $Cl_3(H_2O)Sn(acac)\cdot H_2O$: C = 16.76 wt %, H = 3.08 wt %; Found C = 16.67 wt %, H = 3.04 wt %), which looks like monomers of trichlorohydro(2,4-pentanedionato)tin(IV) monohydrate (Figure 6a). The asymmetric unit contains four monomers bridged together by hydrogen bonding, developing an infinite polymeric structure parallel to the (001) crystallographic planes, as shown in the ORTEP[39] projection at Figure 6b. The oxygen atoms of the bidentate acac ligand are located at 2.063 ± 0.005 and 2.078 ± 0.005 Å of the tin atom. The other four positions of the distorted octahedral coordination of tin(IV) atom are occupied by the three Cl atoms at mean distances of 2.36 Å and by the O of the bonded water molecule, at 2.150 ± 0.005 Å. The relevant structural parameters so determined are gathered in Tables 2 and 3, grouped with the hydrogen bond lengths and angles, while other relevant crystallographic parameters are deposed at the Cambridge Crystallographic Data Center with CCDC 193964. The intramolecular distances are analogous to that reported for the $Cl_2Sn(acac)_2$[12] and are totally consistent with the EXAFS parameters determined for the first coordination shell of tin species in Ac6 solution after addition of water (Ac6, $h = 105$).

Table 2. Crystallographic Data for the Complex C100−Ac6

formula	$C_5H_9Cl_3O_3\,Sn\,H_2O$
formula weight	360.20
crystal system	Monoclinic
space group	$P2_1/c$
unit cell dimensions:	
a (Å)	7.408(1)
b (Å)	6.980(8)
c (Å)	23.867(3)
β (deg)	94.39(1)
unit cell volume V (Å^3)	1231(1)
no. of formula units per unit cell Z	4
calcd crystal density D(calc) (Mg/m^3)	1.944
absorption coefficient μ(Mo Kα) (mm^{-1})	2.711
total no, of electrons in the unit cell F(000)	696
crystal size (mm)	0.15 × 0.20 × 0.25
temperature (K)	293
radiation wavelength Mo Kα (Å)	0.71073
θ min−max (deg)	2.8, 30.0
data set hkl min:max	−10:10; −2:9; −33:21
no of reflctns, total, unique data	4568, 3578
internal reliabitlity factor R(int)	0.062
observed data [$I > 2\sigma(I)$]	2125
no. of reflctns: N_{ref}, no. of params used in the refinement N_{par}	3578 126
reliability factor R	0.0575
weighted reliability factor $wR2$	0.1795
goodness of fit S	1.00
$w = 1/[\sigma^2(F_o^2) + (0.0990P)^2 + 0.5295P]$, where $P = (F_o^2 + 2F_c^2)/3$	
max and av shift/error	0.00, 0.00
min and max residual density (e/Å^3)	−0.92, 1.18

Effect of AcacH/Sn Ratio on the Composition of Thermohydrolyzed Solutions. The evolution of the PRDFs observed for the solutions as a function of the acacH/Sn ratios can be explained by a partial condensation of soluble tin species to form SnO_2 nanoparticles. Tin atoms in solution are mainly involved either in the SnO_2 nanoparticles or in the soluble tin species eventually complexed by acac. Then we have reproduced the filtered EXAFS signals in solution after thermohydrolysis by a weighted linear combination of the filtered EXAFS signals of SnO_2 nanoparticles obtained after dialysis and freeze-drying and of the initial solution before heating ($h = 105$). Figure 7 displays the best linear combinations so obtained; the percentages of the two components so fitted are also indicated, evidencing as a trend that the presence of acacH at high concentration (Ac6 and Ac4) drastically affects the SnO_2 formation by thermohydrolysis. On the other hand, the composition of the solutions after 120 min of thermohydrolysis appears relatively unchanging for acacH/Sn ≤ 2, i.e., ∼27% of SnO_2.

Discussion

We have shown that the solution at the advanced stages of the thermohydrolysis is a mixture of soluble tin species and SnO_2 nanoparticles. The trend evidenced by linear combinations between the filtered EXAFS spectra at the early stage of hydrolysis and of those of SnO_2 nanoparticles to reproduce the filtered EXAFS signals of thermohydrolyzed solutions is a decrease of

(39) Farrugia, L. J. ORTEP3 for windows. *J. Appl. Cryst.* **1997**, *30*, 565.

(40) Séby, F.; Potin-Gautier, M.; Giffaut, E.; Donard, O. F. X *Geochim. Cosmochim. Acta* **2001**, *65*, 3041.

Table 3. Distances (Å) and Angles (deg) for the Complex C100−Ac6 and Hydrogen Bonds (Å) and Angles (deg) for the Complex C100−Ac6

	Sn	Cl1	2.355(4)	C1	C5	1.481(9)	
	Sn	Cl2	2.342(3)	C1	C2	1.371(9)	
	Sn	Cl3	2.382(3)	C2	C3	1.401(9)	
	Sn	O1	2.078(5)	C3	C4	1.508(9)	
	Sn	O2	2.063(5)	O1	C1	1.300(8)	
	Sn	O3	2.150(5)	O2	C3	1.289(8)	
	O3	H13O	0.73(8)	O3	H23O	0.71(12)	
	O1W	H2OW	0.76(9)	O1W	H1OW	0.75(11)	
Cl1	Sn	Cl2	100.15(8)	Cl2	Sn	O3	85.8(1)
Cl1	Sn	Cl3	96.93(8)	Cl3	Sn	O1	86.0(1)
Cl1	Sn	O1	92.7(1)	Cl3	Sn	O2	170.1(1)
Cl1	Sn	O2	90.3(1)	Cl3	Sn	O3	88.5(1)
Cl1	Sn	O3	171.4(2)	O1	Sn	O2	86.8(2)
Cl2	Sn	Cl3	96.05(7)	O1	Sn	O3	81.0(2)
Cl2	Sn	O1	166.6(1)	O2	Sn	O3	83.6(2)
Cl2	Sn	O2	89.4(1)				
Sn	O1	C1	125.5(4)	Sn	O2	C3	126.2(4)
O1	C1	C2	124.9(6)	O1	C1	C5	115.1(6)
O2	C3	C4	115.9(6)	O2	C3	C2	124.5(6)
C2	C1	C5	120.0(6)	C1	C2	C3	126.8(6)
C2	C3	C4	119.6(6)				
H13O	O3	H23O	123(8)	H1OW	O1W	H2OW	108(9)

1[a]	2[b]	3[c]	d12	d23	d13	angle 123
O1W	H1OW	Cl3[1]	0.75(11)	2.53(10)	3.234(7)	159(9)
O1W	H2OW	Cl3[2]	0.76(9)	2.71(9)	3.286(7)	134(8)
O1W	H2OW	O1[2]	0.76(9)	2.30(9)	2.980(8)	150(9)
O3	H13O	O1W[3]	0.73(8)	2.00(8)	2.683(8)	159(9)
O3	H23O	O1W	0.71(12)	2.03(11)	2.734(8)	170(8)

[a] $1 = 2 - x, -1/2 + y, 1/2 - z$. [b] $2 = x, -1 + y, z$. [c] $3 = 1 - x, 1/2 + y, 1/2 - z$.

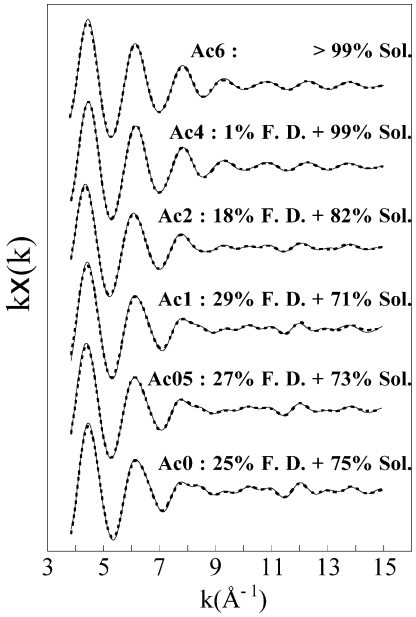

Figure 7. Filtered EXAFS signals of the thermohydrolyzed solutions ($t = 120$ min) (dotted line) for the different acacH/Sn amount reproduced by linear combinations (full lines) of the filtered EXAFS spectrum recorded for the freeze-dried powders and of the filtered EXAFS spectrum recorded for the $h = 105$ and $t = 0$ solution.

the amount of nanocrystalline SnO_2 obtained after 120 min of thermohydrolysis at 70 °C with the increase of AcacH in solution. This indicates that acetylacetone acts as delaying agent for the nucleation (hydrolysis) process involved in SnO_2 particles formation. But it does not change the condensation process since the average crystallite size (2 nm) is not affected by the acacH/Sn ratio. A similar behavior for the invariance of size was already reported in ref 7 for the hydrolysis of tin isopropoxide in the presence of acacH followed by aging at 60 °C for 24 h. The results presented herein are fully in agreement with our previous in situ SAXS study.[19] Both works suggest comparable reactivity for the hydrolyzed species involved in the condensation reaction whatever the acacH/Sn ratio used in initial solution. However, the amount of so-obtained colloidal SnO_2 particles decreases drastically for acacH/Sn > 2. Taking into account this behavior, the discussion will be focused on clarifying two main aspects: first, the change of nature of molecular precursor with the acacH content in the initial solution before and after water addition and, second, the mechanism of the initial step of the formation of SnO_2 nanoparticles. For the sake of clarity, we will discuss first the results concerning the precursors prepared with excess of acacH and in the following those with acacH/Sn < 2.

For acacH/Sn ≥ 2, the mean coordination numbers (Table 1) found for oxygen ($N_{Sn-O} \approx 2$) and chlorine atoms ($N_{Sn-Cl} \approx 4$) in the first coordination shell of tin in solutions with $h = 5$ are in agreement with the presence of anhydrous monochelate, like the monomeric species $[Cl_4Sn(acac)]^-$. This molecular unit formation is also in agreement with the ESI-MS, and NMR results evidence the dominant formation of monomeric monochelate species. The changes of the mean coordination number ($N_{Sn-O} \approx 3$ and $N_{Sn-Cl} \approx 3$) just after the addition of water ($h = 105$) at RT can be accounted by the first step of hydrolysis and formation of hydrated monochelate $Cl_3(H_2O)Sn(acac)$ having the monomeric structure of isolated single crystal (Figure 6a). However, NMR shows clearly the presence of a second different chelate species (Figure 5b) besides the monomeric monochelate species. Its heavy molecular mass species (m/z 446) and the existence of a medium-range order ($R > 2.2$ Å) around Sn atoms in its EXAFS spectrum

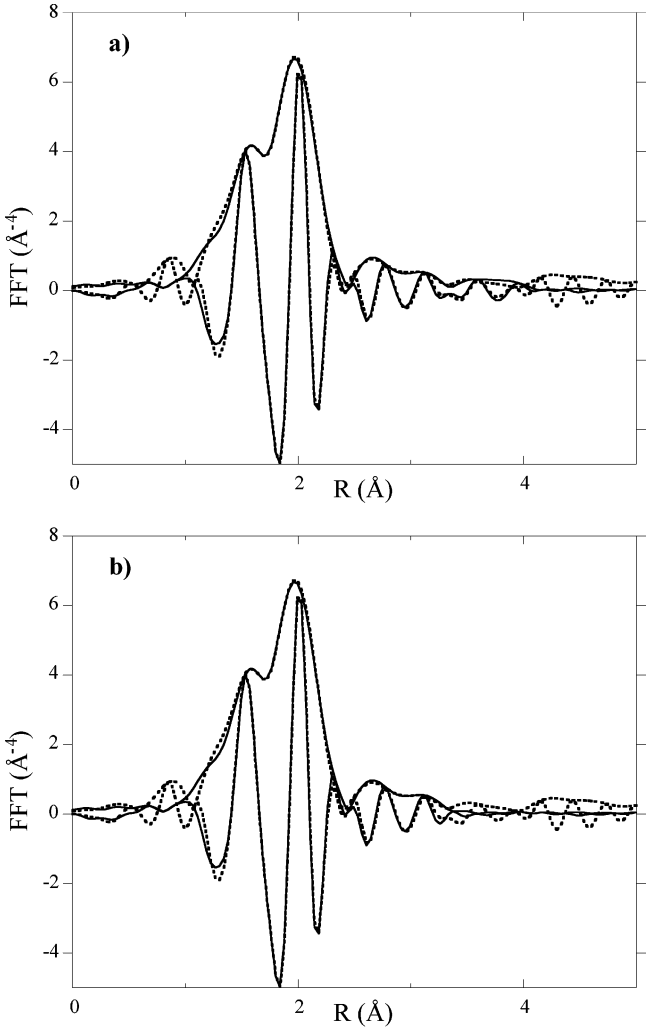

Figure 8. FeFFIT simulations of the EXAFS spectrum of the Ac6, $h = 105$ solution (before heating). (a) Simulation performed considering a Sn−Sn* contribution; (b) simulation performed without the Sn−Sn* contribution. These simulation are based on the $Cl_3(H_2O)Sn(acac)$ molecule shown in Figure 6a, with unchanged distances between the absorbing Sn atom and the atoms of the acac ring. Sn−O (for O belonging to the water molecule), Sn−Cl, and Sn−Sn*, if any, distances are only refined. The parameters used for the simulations are gathered in Table 4 of Supporting Information.

(Figure 2) suggest the formation of small polycationic species (dimer, trimer, ...). The formation of such cationic species was confirmed by evidencing the presence of Sn second neighbors around the absorbing atom from ab initio FeFFiT simulations of the EXAFS spectrum of Ac6, $h = 105$ (before heating). The distances of the first coordination shell (made of three chlorine atoms and three oxygen atoms, two from acac ligand and one from aquo ligand) were fitted whereas the Sn−C distances were kept fixed at the values reported for the $Cl_3(H_2O)Sn(acac)\cdot H_2O$ crystal. The same multiple scattering contributions as those used for the reproduction of $Cl_3(H_2O)Sn(acac)\cdot H_2O$, up to a total half-effective length of 4.0 Å, were considered. Panels a and b of Figure 8 show the simulations performed with and without a Sn−Sn contribution, respectively. The small peak at ∼3.6 Å is satisfactorily reproduced, taking account of a tin atom located at 3.95 Å from the absorbing atom. The EXAFS parameters determined by the fitting procedure for the simulation of the EXAFS spectra of $Cl_3(H_2O)Sn(acac)\cdot H_2O$ and of Ac6, $h = 105$ (before heating), were reported in Table 4 given in the Supporting Information. They are consistent with the formation of polycationic species. In fact, it is expected that the equilibrium between the monomeric and the oligomeric complex is easily displaced by the change of the reactant concentration and the addition of water as previously reported by Chandler[10] for the acac-modified tin alkoxide. Although, the thermodynamic constants for this class of tin(IV) complex are unknown,[40] making difficult the modeling of this equilibrium, the abundance of the oligomeric species when water is added strongly suggests that tin atoms are linked by one hydroxo or oxo bridge. In this framework, the addition of water and subsequent equilibrium between monomeric and oligomeric species should be for Acac/Sn = 6:

$$[Cl_4Sn(acac)]^- + H_2O \rightarrow [Cl_3Sn(acac)(H_2O)] + Cl^- \leftrightarrow [Cl_3(acac)Sn(\mu_2\text{-}OH)]_2^- + HCl$$

Note that without further substitution of chlorine ligand by water the oligomerization is limited to the formation of dimers.

A 5-fold coordination shell for tin with $N_{Sn-O} \approx 1$ and $N_{Sn-Cl} \approx 4$ was determined by EXAFS for the precursor in initial ethanolic solution without the addition of acacH and water (Ac0, $h = 5$). Possible models for this precursor should be monomeric $[Cl_4Sn(H_2O)]$ or $[Cl_4Sn(EtOH)]$ species, but oligomeric species cannot be excluded. The low coordination number for tin observed in the Ac0 sample ($h = 5$) favors the nucleophilic addition[1] of water in order to fit the stable 6-fold coordination. As revealed by EXAFS, upon addition of water ($h = 105$), a partial substitution of the terminal hydrolyzable Cl ligand by Sn−O bonds are clearly evidenced by the decrease of the N_{Sn-Cl} from 4.4 to 2.6 and the increase of the N_{Sn-O} from 0.8 to 3.3. Thus, the driving forces of hydrolysis are 2-fold: the expansion of the coordination number from 5 to 6 and the substitution of chlorine ligand by water. The presence of water molecules in the coordination sphere of tin favors the beginning of condensation as indicated by the Sn−Sn contribution located at ∼3.6 Å on the PRDF of Ac0, $h = 105$ (Figure 2 a). Ab initio simulations of the EXAFS spectrum of Ac0, $h = 105$, performed in the same way as previously described for Ac6 $h = 105$ (Figure 8) was successfully reproduced with a minimization of the distance between tin atoms at 4.00 Å evidencing the formation of oligomers. As no remarkable change of quasi-elastic light scattering was observed after water addition at RT, we assume the formation of small oligomers such as dimer, trimer, etc.

It is noteworthy that, as the acacH content increases, the total tin coordination number for the first coordination sphere in initial ethanolic solutions without water addition ($h = 5$) does not change drastically (from 5.2 to 5.4). Thus, the remarkable increase of N_{Sn-O} coordination number from 0.8 to 1.7 and decrease of N_{Sn-Cl} coordination number from 4.4 to 3.7 indicates that one acacH molecule substitutes water (or EtOH) ligands and partially hydrolyzable chlorine ligands. However, the fact that the N_{Sn-O} coordination number is systematically lesser than 2 indicates a mixture of unchelate and

chelate acac species. The addition of water leads to the expansion of the coordination sphere of tin toward the 6-fold coordination and the partial substitution of chlorine ligands. Favorable conditions for polycondensation reactions are then reached; nevertheless, the formation of SnO_2 particles at RT is only evidenced by EXAFS for Ac0 and Ac05. This suggests that the formation of nanoparticles is strongly related to the relative proportions of unchelate and chelate acac species in solution. For excess of acetylacetone, i.e., acacH/Sn > 2, the condensation is limited to the formation of small oligomeric species, like the proposed dimer for Ac6, $h = 105$.

Finally the excess of acetylacetone, acacH/Sn > 2, is a prerequisite to the formation of a tin−acac−chelate complex at RT and stabilizes the precursor against the formation of SnO_2 nanoparticles at 70 °C. This behavior can be due to the equilibrium between bonded acac and free acacH that is displaced toward complexation as the acacH/Sn ratio in the reaction bath increases. Furthermore, the increase of temperature also favors the complexation reaction and the increase of the content of tin chelate species.[10] Then the stability of less hydrolyzable acac chelate ligand during the thermohydrolysis at 70 °C for 120 min accounts for the low amount of SnO_2 nanoparticles (Figure 7) formed for acacH/Sn > 2.

Conclusion

The structure of molecular species present in tin tetrachloride ethanolic solution containing different amounts of acetylacatonate as complexing ligand was reported. The RT formation of monochelate acac tin complex is systematically verified. But the proportion of this chelate species increases with the acacH/Sn ratio. Whatever the acacH/Sn ratio, an expansion of the tin coordination sphere from 5 to 6 is evidenced upon addition of water at RT, which allows the occurrence of polycondensation reactions. In these conditions, condensation reactions are limited to the formation of small oligomeric species in excess of acetylacetone (acacH/Sn > 2).

Single crystals were isolated from the solution with AcacH/Sn = 6 and nominal hydrolysis ratio of 105. The structure is built up from monomeric $Cl_3(H_2O)Sn(acac)\cdot H_2O$ units bridged together by hydrogen bonding. But in solution, these monomeric units are in equilibrium with dimeric species, with possible $[Cl_3(acac)Sn(\mu_2\text{-}OH)]_2^-$ arrangement.

The size (2 nm) of the SnO_2 nanoparticles formed by thermohydrolysis is independent of the acacH content in the reaction bath. In the presence of an excess of acacH (acacH/Sn > 2), the hydrolytic stability of the acac−chelate complex increases, preventing the progress of further condensation reaction and resulting in less than 1% of nanoparticles. On the contrary, for acacH/Sn < 2, the amount of SnO_2 nanocrystalline particles obtained by thermohydrolysis is similar to that obtained with the solution without acacH (∼27%).

Acknowledgment. This work has been financially supported by FAPESP and CNPq (Brazil) and by a CAPES/COFECUB grant. The authors are grateful to L. Broussous for preparation advice and M. Furlan for providing the ESI-MS facility.

Supporting Information Available: Table 4, scattering paths and parameters used in the FeFFIT simulations of the $Cl_3(H_2O)Sn(acac)\cdot H_2O$ single crystal and of Ac6, $h = 105$ (before heating). This material is available free of charge via the Internet at http://pubs.acs.org.

CM040141Q